Wellbore-Stability Study for the SAFOD Borehole Through the San Andreas Fault

Pijush Paul,* SPE, and **Mark Zoback,** SPE, Stanford University

Summary

This paper presents a wellbore-stability study of the San Andreas Fault Observatory at Depth (SAFOD) research borehole located near Parkfield, California, USA. In the summer of 2005, the SAFOD borehole was drilled successfully through the active trace of the San Andreas Fault (SAF) in an area characterized by fault creep and frequent microearthquakes. In this study, we report how the analysis of wellbore failures in the upper part of the hole, geophysical logs, and a model for stress gradients in the vicinity of the fault were used to estimate the mud weights required to drill through the fault successfully. Because logging-while-drilling (LWD) acoustic caliper data and real-time hole-volume calculations both showed that relatively little failure occurred while drilling through the SAF, the predicted mud weight was successful in drilling a stable borehole. However, a six-arm caliper log, run after drilling was completed, indicates that there was deterioration of the borehole with time, which appears to be caused by fluid penetration around the borehole. The LWD-resistivity measurements show that essentially no fluid penetration occurred as the hole was being drilled. Because of this, the mud weight used was capable of maintaining a stable wellbore. However, the resistivity data obtained after drilling show appreciable fluid penetration with time, thus negating the effectiveness of the mud weight and leading to time-dependent wellbore failure. Using finite-element modeling (FEM), we show that mud penetration into the fractured medium around the borehole causes failure with time.

Introduction

Drilling perturbs the stress state around a well, and wellbore-stability problems can occur when the near-wellbore stresses substantially exceed the strength of the rock. Excessive instability around a wellbore can be suppressed by choosing an optimally stable borehole orientation and sufficiently high mud weight. Some types of wellbore-wall failure, such as key seating, usually do not cause instability in the borehole but can exacerbate failure in an already unstable borehole.

As described below in the paper, drilling through the SAF in the SAFOD project was conducted in various phases. In this paper, we discuss an analysis of wellbore failures after the first phase of drilling in order to predict the mud weight required to drill successfully through the SAF during the second phase of the project. The main challenges during the SAFOD drilling were the unknown stress field and rock strength along the planned drilling trajectory. Hence, to estimate the mud weight to be used for drilling the SAF zone, we first calibrated a theoretical-stress model (Chéry et al. 2004) for the SAF with the observed borehole failures and minifrac-test data of the first phase of drilling. Then, we estimated and calibrated a uniaxial-compressive-strength (UCS) profile for the rocks encountered by modeling the severity of borehole failures, allowing for a wide range of expected rock strengths because of the possibility of extensive damage to the rocks caused by earthquakes on the SAF.

As will be shown, LWD-caliper data during the second phase of drilling show successful drilling through the SAF using the estimated mud weights inferred from the geomechanical model. However, wireline calipers were enlarged at the top section of the borehole, indicating severe failure with time. We use FEM to show the borehole failure with time. Block theory (Goodman 1989; Goodman and Shi 1985), used for the stability of underground openings, suggests that only the removable blocks of the top section fail because of gravity, but the lower section remains in gauge despite having removable blocks. This explains why the time-dependent enlargement of the SAFOD borehole is restricted to only the top section of the hole.

The SAF and the SAFOD location

The SAF is a transform fault that is the principal zone of deformation accommodating relative motion between the Pacific and North American plates. The Pacific plate moves ≈48 mm/a to the northwest relative to the North American plate. The SAFOD well is located near Parkfield, roughly halfway between San Francisco and Los Angeles **(Fig. 1).** The drillsite is on a segment of the SAF that moves through a combination of aseismic creep and repeating microearthquakes. In the vicinity of the drillsite, nearly all the slip on the fault is aseismic, with the many small earthquakes contributing little to the overall slip rate.

The SAFOD borehole is located on the west side of the SAF where the bedrock was expected to be mostly granitic at depth, with rocks associated with the Franciscan formation expected on the eastern side of the fault. In fact, the geology turned out to be more complicated than this, with arkosic sandstone and conglomerates (derived from the granites) on the west side of the fault and most of the formations encountered on the east side of the San Andreas consisting of the Great Valley formation (Boness and Zoback 2006). The fault zone itself is presumed to consist of crushed breccias and fault gouges. The width of the zone of intense deformation at depth (i.e., the SAF zone itself) and that of the damage zone surrounding the fault were unknown before drilling.

The SAFOD-Drilling Plan

The SAFOD project was carried out in multiple phases. As shown in **Fig. 2,** a vertical pilot hole, located 1.8 km to the southwest of the SAF, was drilled in 2002 and encountered granitic rock at ≈850 m as predicted by geophysical data. The design of the main SAFOD borehole was to drill vertically at the same drillsite as the pilot hole to a depth of ≈1.5 km and then drill a deviated hole through the fault zone in the vicinity of microearthquakes (magnitude ≈2 and smaller) located by Thurber et al. (2004). In the summer of 2004, Phase 1 was completed to a measured depth (MD) of 3,048 m. After Phase 1, the borehole was logged, cased, and cemented, and a seismic study was carried out in the borehole to improve knowledge of subsurface velocities and the location of the target microearthquakes. Using this information, Phase 2 was carried out during the summer of 2005. The study reported here describes how we used data from Phase 1 to predict an optimum mud weight for drilling through the SAF in Phase 2. Conventional rotary drilling was used for Phases 1 and 2, and extensive cuttings samples were collected; sophisticated gas sampling was performed in real time, and comprehensive geophysical logging was carried out. Having obtained this information through the SAF zone, multilateral core holes were drilled through the fault zone in the summer of 2007 (Phase 3).

The vertical section of the Phase 1 borehole was drilled mostly with a 17½-in. bit and cased with 13⅜-in. casing. The deviated interval of the well (from 1.5 to 3 km MD) was drilled with a

* Now with ConocoPhillips.

This paper (SPE 102781) was accepted for presentation at the 2006 Annual Technical Conference & Exhibition, San Antonio, Texas, USA, 24–27 September, and revised for publication. Original manuscript received for review 22 June 2006. Revised manuscript received for review 20 May 2008. Paper peer approved 15 June 2008.

Fig. 1—The SAFOD borehole is located near Parkfield Califonia, on a segment of the SAF that shows aseismic creep and repeating microearthquakes (map from US Geological Survey) (M=magnitude).

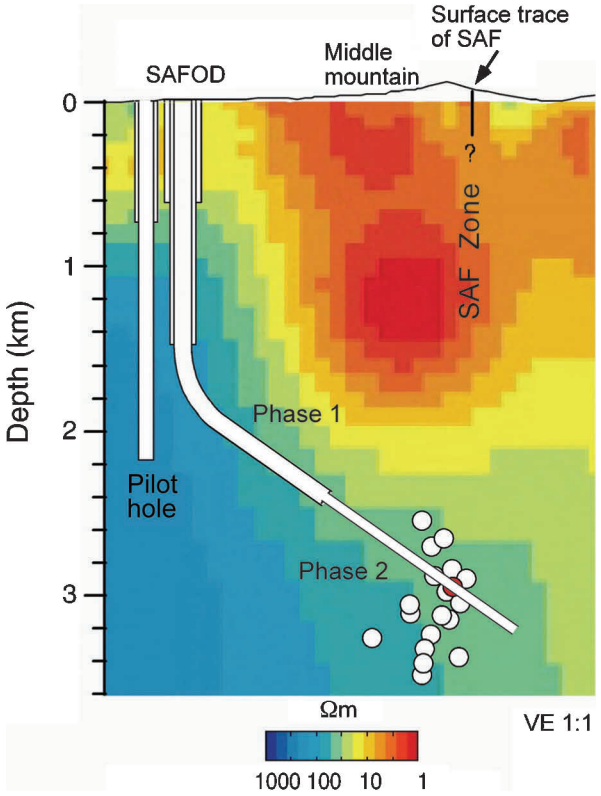

Fig. 2—A schematic of the SAFOD well trajectory superimposed on resistivity section determined from inversion of active source magneto-telluric data (Unsworth and Bedrosian 2004).

12¼-in. bit and completed with 9⅝-in. casing. The 54° deviation of the hole was achieved with a build rate of 2.5° per 30 m. Phase 2 was drilled from 3.05 km MD to 3.8 km MD with an 8½-in. bit and was completed with 7-in. casing (Zoback 2006).

Borehole Stability and Lithofacies for Phase 1

As interpreted from well-log analysis, three major lithofacies are intersected by the SAFOD well during Phase 1 (Boness and Zoback 2006). As shown in **Fig. 3,** the first 800 m consists mostly of weathered Tertiary sediments. This is followed by fractured granite and granodiorite to 1926 m MD. Below that, sedimentary rocks (interpreted to be made up of arkosic sandstone with interbedded shale and conglomerate) were encountered down to 3048 m. These sedimentary rocks were not predicted by geological or geophysical models before drilling. Phase-1 borehole-resistivity-image logs [using a Fullbore Formation MicroImager (FMI) (Schlumberger 2004)] indicate numerous natural fractures and faults throughout the entire interval drilled, and bedding in the sedimentary section. In conjunction with the other geophysical logs and cuttings analysis, a number of faults and brecciated zones were identified.

In general, there were relatively few problems during Phase-1 drilling, even in the fault zones, although a number of trips were needed to wash and ream the hole at several depths. In **Fig. 4,** maximum and minimum diameters calculated from either the density caliper or the FMI dual-caliper log are presented to show the overall condition of the hole. The hole size in the sedimentary zone above 850 m (that was logged only from 650 to 850 m) is enlarged on all sides of the borehole. There is a slight improvement in hole condition in the upper, weathered granite (850–1000 m), but most of the granite/granodiorite section is generally in gauge. The granodiorite section from 1440 m to 1920 m shows only a slight enlargement of the borehole diameter. In the fault zone at the granite/sediment contact at 1920 m, we observe significant hole enlargements, again on all sides of the hole. Significant hole enlargements also are seen in the sedimentary section below 1,926 m, especially at some depth intervals. Better hole conditions are observed in the sandstone interval starting at 2682 m.

At depths below 1440 m, a detailed analysis of the caliper data reveals the orientation of borehole elongations that are ≈10° counterclockwise from the top and bottom of the hole (Fig. 4). The fact that the borehole enlargements are close to the top and bottom of the hole suggests that they might be caused by key seating. This is discussed in more detail in the next section.

Stress Analysis

The SAF has been described as having low frictional strength because many in-situ-stress measurements show a high angle between the direction of the maximum principal horizontal stress ($S_{H\max}$) and the strike of the fault (Zoback et al. 1987; Mount and Suppe 1987; Townend and Zoback 2004; Provost and Houston 2003; Hickman and Zoback 2004) and the absence of frictionally generated heat (Brune et al. 1969; Lachenbruch and Sass 1980). We developed a preliminary stress-distribution model for the well trajectory on the basis of a geodynamic model of Chéry et al. (2004) (**Fig. 5**) that proposes that the SAF has a very low intrinsic friction coefficient ≈0.1. The possibility that the fault is characterized by anomalously high pore pressure (Rice 1992) would, in effect, produce very similar results, but no evidence for high pore pressure was found during drilling (Zoback et al. 2007). The Chéry et al. model (2004) divides the region into a near field (NF) (within ≈5 km of the fault) and the core of the fault zone (FZ) itself. The model predicts how stress magnitudes and the orientation of $S_{H\max}$ vary with depth and with distance to the fault. This model predicts that the shear stress on planes parallel to the fault zone is very low and varies strongly with both distance to the fault and with depth.

Close to the SAF (in the NF), Chéry et al. (2004) proposed that the minimum principal stress (S_3) is close to the vertical stress (S_v). The maximum principal stress (S_1), which is equivalent to $S_{H\max}$ is approximately two times the vertical stress. This stress state implies a strike-slip-/reverse-faulting regime (Anderson 1951) with magnitudes consistent with Coulomb's theory of faulting for laboratory-determined coefficients of friction and hydrostatic pore pressure (Zoback 2007). In the model, the maximum horizontal stress, $S_{H\max}$, is oriented N30°E, which is at a high angle to the SAF. The minimum and maximum principal stresses are in a ver-

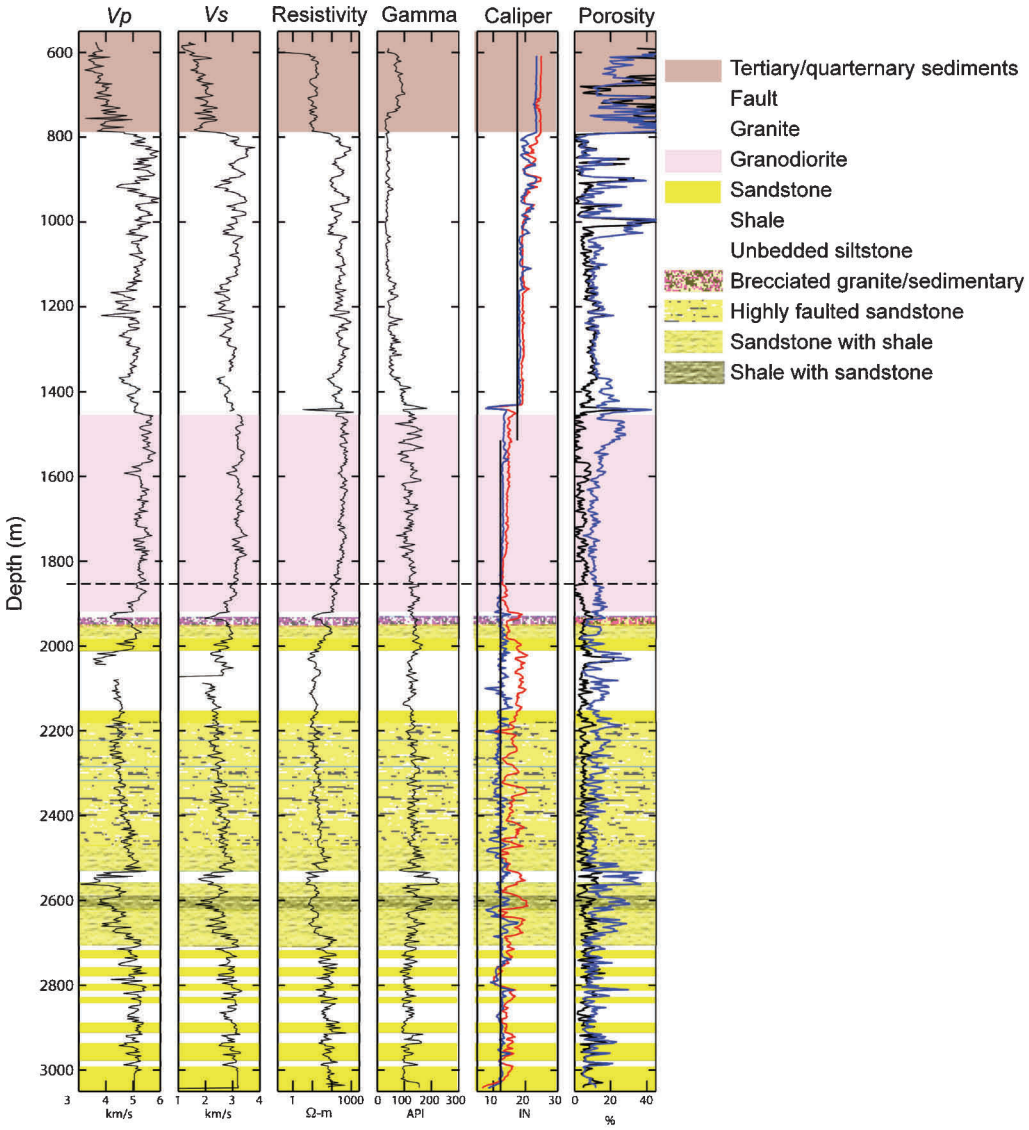

Fig. 3—A simplified lithology column calculated using petrophysical logs collected during the Phase-1 drilling of the SAFOD borehole (Zoback 2006).

tical plane almost perpendicular to the SAF and cause reverse faulting on faults, striking parallel to the SAF. However, the calculated normal stress acting on the FZ is close to $S_{H\max}$. This stress state is essentially identical to that measured in the SAFOD pilot hole to 2-km depth (Provost and Houston 2003). Within the FZ, the Chéry et al. model (2004) predicts that all three principal stresses are nearly equal and close to twice the lithostatic stress, S_v, (i.e., $S_1 \approx S_2 \approx S_3 \approx 2 \cdot S_v$). A theoretical model by Rice (1992) also supports this dramatic change in the value of S_3 from the NF to FZ (Lachenbruch and Sass 1980).

For this study, we obtained the lithostatic stress from density logs and other densities derived from gravity models in the drillsite area. The Chéry et al. model (2004) was then used to estimate principal stresses in the NF and FZ from the lithostatic-stress gradient. We used linear interpolation to define the distribution of the stress between the NF and FZ and assumed a 300-m-thick FZ that is symmetric about the surface trace of the fault. Stress and pore-pressure models in the well-trajectory plane are shown in **Fig. 6.** To be consistent with the observations made in the pilot hole (Provost and Houston 2003), the azimuth of $S_{H\max}$ varies with depth. The high value for S_3 predicted by the Chéry et al. model (2004) was supported by a minifrac test performed at 3028.5 m MD (the bottom of the casing that was set after completion of Phase 1 at a MD of 3,000 m) and at the onset of Phase-2 operations. The minifrac test was carried out in an openhole interval with highly fractured rock. However, at the maximum obtainable pressure of the used fracturing equipment (≈10 MPa above the vertical stress), it was not possible to extend a hydraulic fracture, implying that the effective minimum principal stress was appreciably above the vertical stress in the tested interval.

The Chéry et al. study (2004) was carried out after the pilot hole was drilled but before Phase-1 drilling. Three observations obtained during Phase 1 led us to slightly revise the preliminary stress model shown in Fig. 6. First, analysis of breakouts, drilling-induced tensile fractures, and dipole sonic logs in the Phase-1 borehole indicates a maximum horizontal-stress orientation of N35°E (Boness and Zoback 2006), which was ≈5°E from that in the preliminary stress model (Chéry et al. 2004). Second, as a result of modifying the velocity model in the vicinity of the San Andreas, there was a shift to the southwest in the microearthquake locations. The result of this is that when Phase-1 drilling was completed, it was clear that the bottom of the hole was within 200 m of the active FZ. Third, the minifrac measurement noted above shows extraordinarily high values of S_3 at the bottom of Phase 1, independently confirming the fact that the active fault is close to the end of Phase-1 drilling and to the southwest of the surface trace.

To constrain stress magnitudes in the arkosic rocks drilled during Phase 1, we modeled the observed borehole failures. **Fig. 7** is a wellbore-stability analysis for wells of any orientation at a true

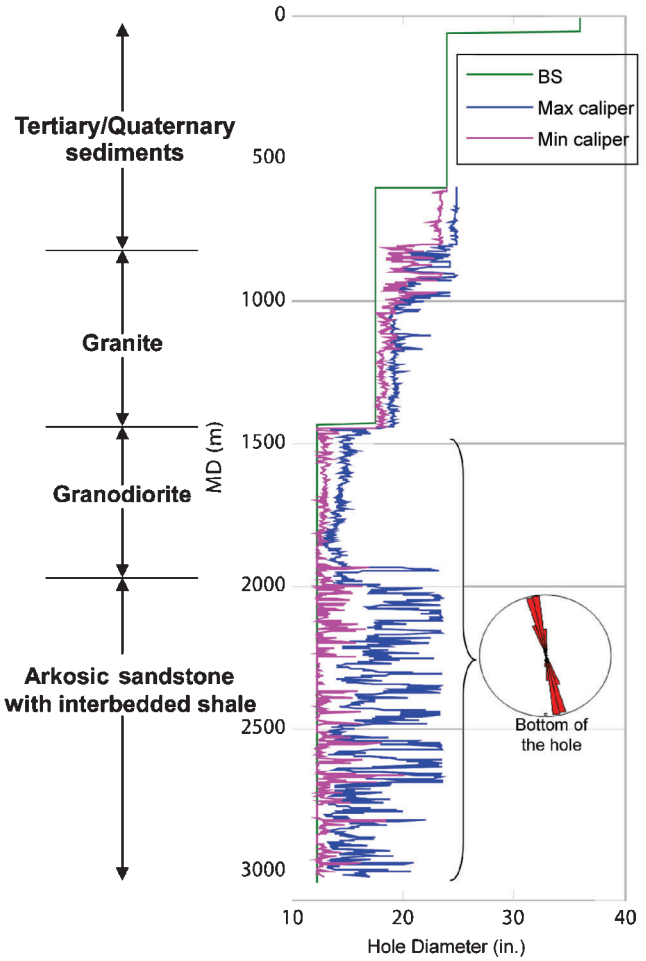

Fig. 4—Maximum and minimum caliper diameters show borehole enlargements during Phase-1 drilling. Below 1440 m, borehole is elongated at ≈10° counterclockwise tilt from the top of the hole (BS=borehole stability).

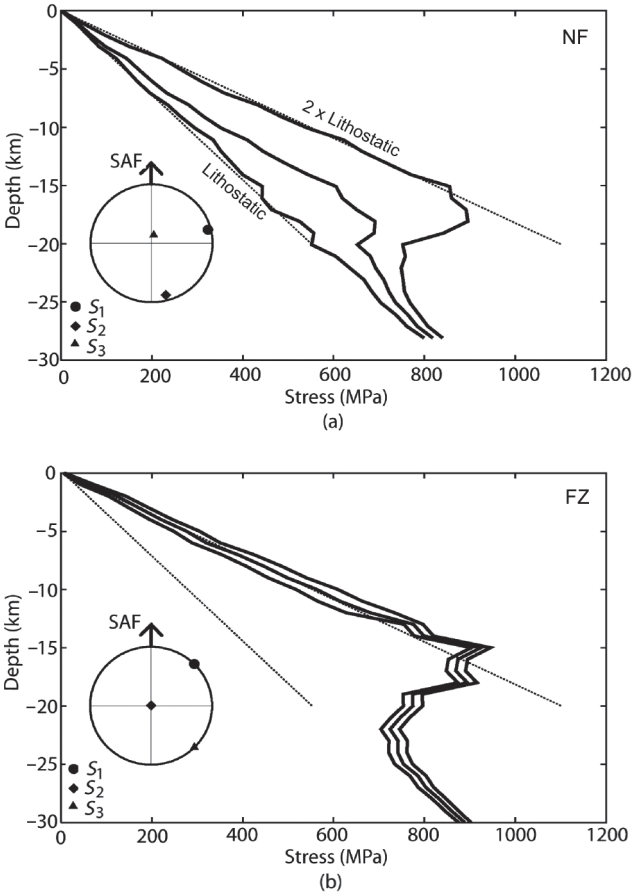

Fig. 5—S_1, S_2, and S_3 profiles with depth and lower-hemisphere stereo plots evaluated at 4-km depth for (a) NF and (b) FZ (Chéry et al. 2004).

vertical depth (TVD) of 2220 m using the methodology described by Peska and Zoback (1995). Radial distance from the center of either diagram in Fig. 7 represents well deviation at a given azimuth. The diagram on the left shows the orientation of a breakout (if it were to form) in a "looking-down-the-hole" coordinate system. The diagram on the right shows the magnitude of rock strength required to prevent failures larger then 60°. The black arrows show the orientation of $S_{H\max}$. The azimuth and orientation of the SAFOD borehole is shown in each diagram. Note that the stress model used (S_1≈101 MPa, S_2≈91 MPa, S_3≈50 MPa, and azimuth of S_1≈N35°E) predicts a breakout orientation that is 10° counterclockwise from the top and bottom of the hole, the same as what was observed in the caliper data (Fig. 4). This exercise shows, therefore, that the observed hole enlargements are stress-induced wellbore breakouts, not key seats, although key seating may exacerbate the depth of the failure zones away from the borehole wall. Although this modified stress model now can be used to constrain in-situ rock strength (Zoback et al. 2003) in the Phase-1 wellbore in the context of the observed failures (Fig. 4), in the next section we first use geophysical logs to constrain rock strength.

UCS Modeling

In cases such as this where no laboratory rock-strength measurements are available, we estimate rock strength by calibrating a best-fit rock-strength model to the nature and severity of borehole failures. For the granite and granodiorite section between 853 and 1926 m, we used a rock-strength model (Eq. 1) of the type proposed by Annor and Jackson (1987), which uses P-wave velocity (V_p) measured from sonic logs to calculate rock strength. This deterministic model was later calibrated for the granite around the SAFOD well by Hickman and Zoback (2004) using pilot-hole data:

$$UCS = 129 + 0.0145V_p, \quad \ldots\ldots\ldots\ldots\ldots\ldots\ldots\ldots\ldots\ldots (1)$$

where UCS is in MPa and V_p is in m/s.

To deal with the uncertainty in rock strength in the diverse sedimentary rocks that were drilled, we compared observed borehole failures with those predicted using several rock-strength models (Chang et al. 2006). These rock-strength models represent a range of sedimentary environments having different values of porosity, cementation factor, clay percentage, and rock strength. We start with a coarse-grained sandstone/conglomerate (Eq. 2) proposed by Moos et al. (2001):

$$UCS = 1.745 \times 10^{-9}\rho V_p^2 - 21, \quad \ldots\ldots\ldots\ldots\ldots\ldots\ldots\ldots\ldots\ldots (2)$$

where UCS is in MPa, bulk density ρ is in kg/m^3, and V_p is in m/s.

We found, however, that the above-described sedimentary-strength model tended to overestimate the rock strength (for estimated stress magnitudes). We believe that the rock is actually weaker than predicted by Eq. 2 because of pre-existing damage and microcracks in the rock (Hoek and Brown 1997; Hoek and Brown 1980; Hongliang and Ahrens 1994; Hu and Huang 1993). Variations of sonic velocity are incapable of completely predicting the zones of increased wellbore failures, nor do density measurements indicate increased porosity associated with faults and fractures in those rocks. Resistivity images and other logs also show no increase of porosity in the failed zone. In this context, we argue that the rock weakness is caused, at least in part, by damage to the rock associated with discrete fractures and faults such that the overall porosity and bulk properties are relatively unchanged.

To incorporate the effect of damage on the rock strength, we use an empirical criterion proposed by Hoek and Brown (1980)

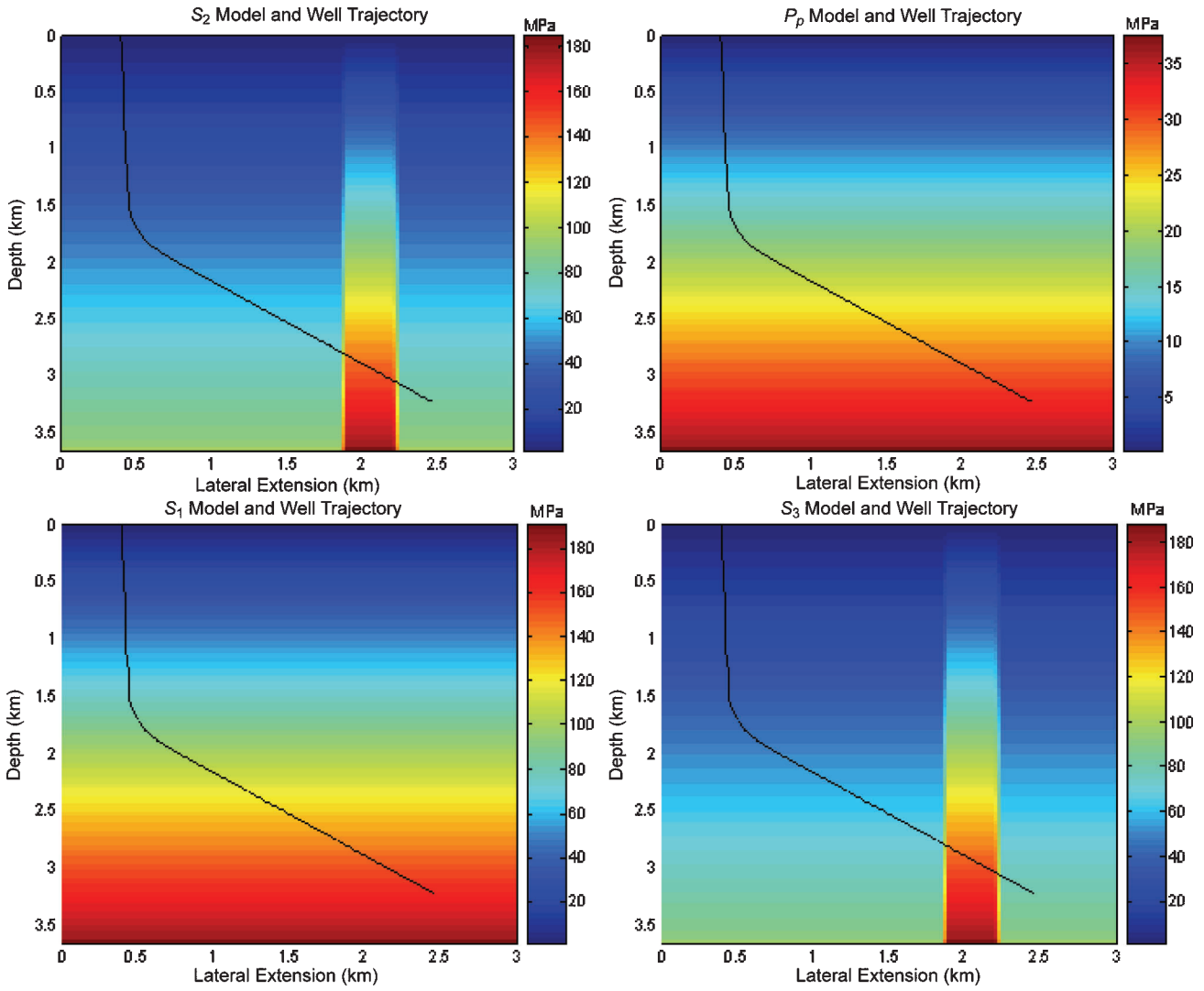

Fig. 6—Three principal stresses, S_1, S_2, S_3, and pore pressure (P_P) on the well-trajectory plane. Black line shows the well path. The anomalous zone in S_2 and S_3 model at 1.8 km of lateral distance shows the SAF zone.

and shown in Eq. 3. It suggests that strength of a rock mass depends on the scale of the damage. A heavily jointed rock mass behaves like an intact rock at fine scale, but at larger scale, it behaves like an isotropic assemblage of interlocking angular particles. Hence, the rock mass will be much weaker at large scale than at fine scale.

The UCS of a jointed-rock mass, UCS_f, is related to UCS of the intact rock, UCS, by Eq. 3.

$$UCS_f = \sqrt{s(UCS)^2}. \quad \ldots\ldots\ldots\ldots\ldots\ldots\ldots\ldots\ldots\ldots\ldots\ldots\ldots\ldots (3)$$

The parameter s in Eq. 3 depends on interparticle tensile strength and the degree of particle interlocking. For an intact rock material $s = 1.0$, for a damaged rock $0<s<1$; and for a completely disaggregated rock, $s = 0$. In other words, s decreases as the degree of fracturing of the rock mass increases because of the greater degree of freedom available to individual pieces of rock material. Laboratory tests on jointed samples of andesite and granite suggest a minimum value as low as 0.0002 for s (Jaeger 1970; Chirkov et al. 2006; Selby 1980). Around the SAFOD borehole, fractures are oriented in all directions, so they do not introduce any intrinsic anisotropy in the rock (Boness and Zoback 2006).

To determine the value of compressive strength of the jointed rock with Eq. 3, we have used the UCS of intact rock calculated from Eqs. 1 and 2 using an empirical approach to estimate the value of s with the dual-caliper measurements. To get an initial approximate value of s, we will assume that if both calipers show that the entire hole is enlarged, we will assume that the breakout has grown into a washout, with the entire circumference of the hole failing. As explained by Zoback (2007), this implies an initial width $\geq 90°$. If one of the caliper pairs shows great enlargement but the other shows an in-gauge hole, then we assume a breakout width $<90°$. If both calipers are in gauge, we assume that the hole has not failed.

In **Fig. 8,** we show the predicted width of breakouts in the SAFOD Phase-1 borehole using the stress model defined for constant rock strengths that vary between 20 and 90 MPa. For rock strengths of 90 MPa, no wellbore failure is seen. When rock strength is ≈80 MPa, only a small amount of failure is observed in the interval 1500–1800 m. Conversely, when strength is as low as 50 MPa, the prediction would be that the entire well below 1300 m would be washed out. One can see, therefore, that realistic rock strengths would appear to be approximately 60–70 MPa for the assumed stress state. This enables us to estimate a value of s that "corrects" the log-derived strength to values consistent with those estimated from the wellbore failures. For the Tertiary section, we found $s \approx 1$ because rock strength predicted by geophysical logs is low enough to model the failure observed during Phase-1 drilling. In the granite/granodiorite section, we found $s \approx 1$, indicating a strong rock whose strength is relatively unaffected by the fractures and faults within it. In the sedimentary section below 1926 m, we found $s \approx 0.85$, which predicts the degree of failure consistent with the observed amount of borehole failure.

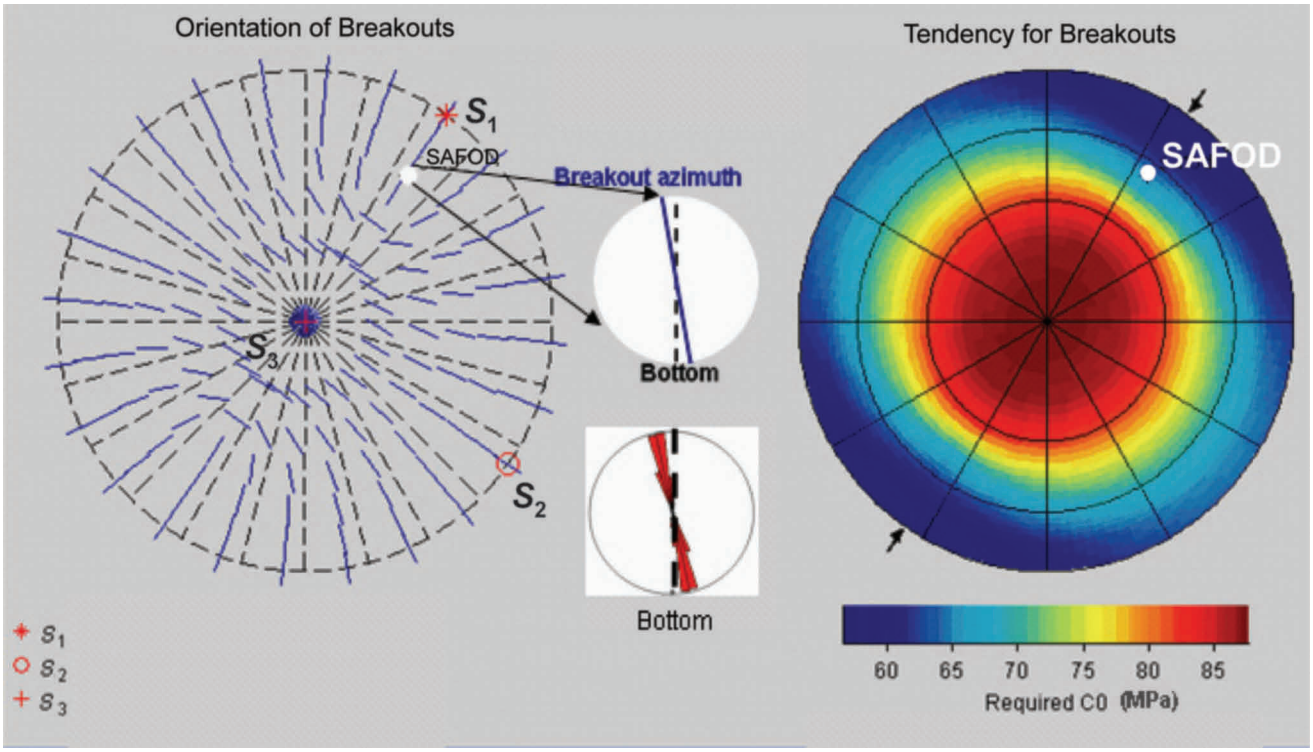

Fig. 7—Modified stress model, with S_{Hmax} azimuth of 35°, $S_{Hmax} \approx 2 \cdot S_v$, $S_{hmin} \approx 1.82 \cdot S_v$, and $S_v \approx$ lithostatic gradient (≈0.025 MPa/m), is able to model breakout azimuth (blue), which matches the orientation of observed borehole enlargements (red).

Modeling of Phase-1 Borehole Failures

To evaluate how well the technique described in the preceding section predicts the degree of wellbore failure observed, we compare the predicted failure width with the actual wellbore failures from the maximum and minimum calipers. We define the breakout width from observed calipers by assuming breakout width less than 90º, if one caliper is in gauge and the other is enlarged. **Fig. 9** shows the minimum and maximum caliper data (Column 1), the predicted strength profile (Column 3), and the theoretical breakout width for $s = 1$ (intact rock), $s = 0.85$ (≈8% weaker than intact rock), and $s = 0.7$ (≈16% weaker than intact rock) in the sedimentary section below 1920 m and for $s = 1$ in sections above 1926 m

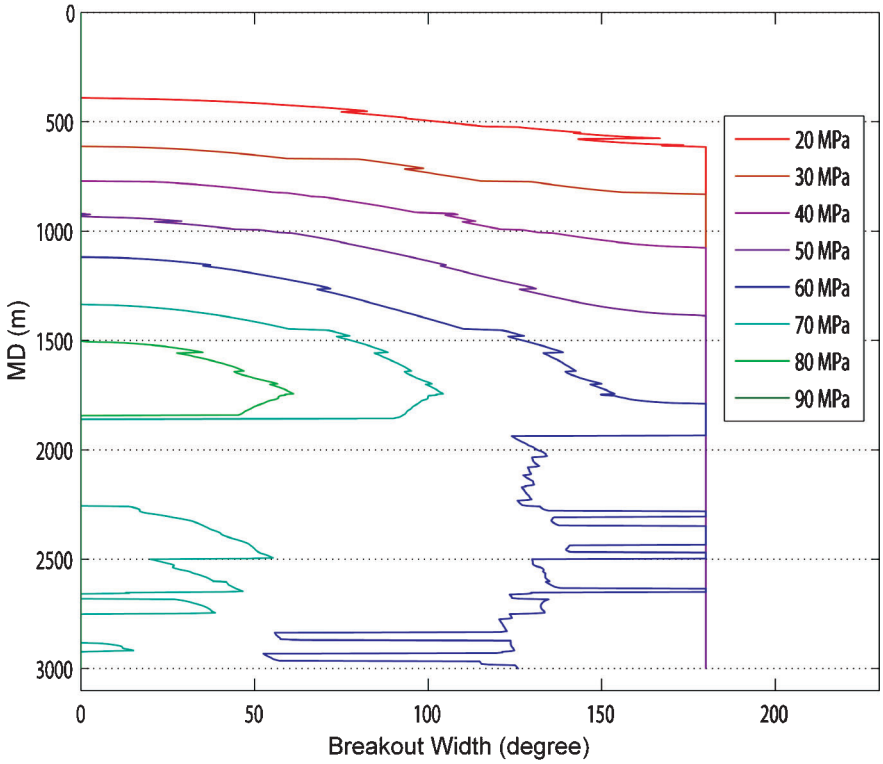

Fig. 8—At 1,920 m to 2,804 m (MD) of the SAFOD well trajectory, deterministic modeling indicates UCS of ≈60–70 MPa for a rock, which gives breakout width ≈90° using mud weight of Phase-1 drilling.

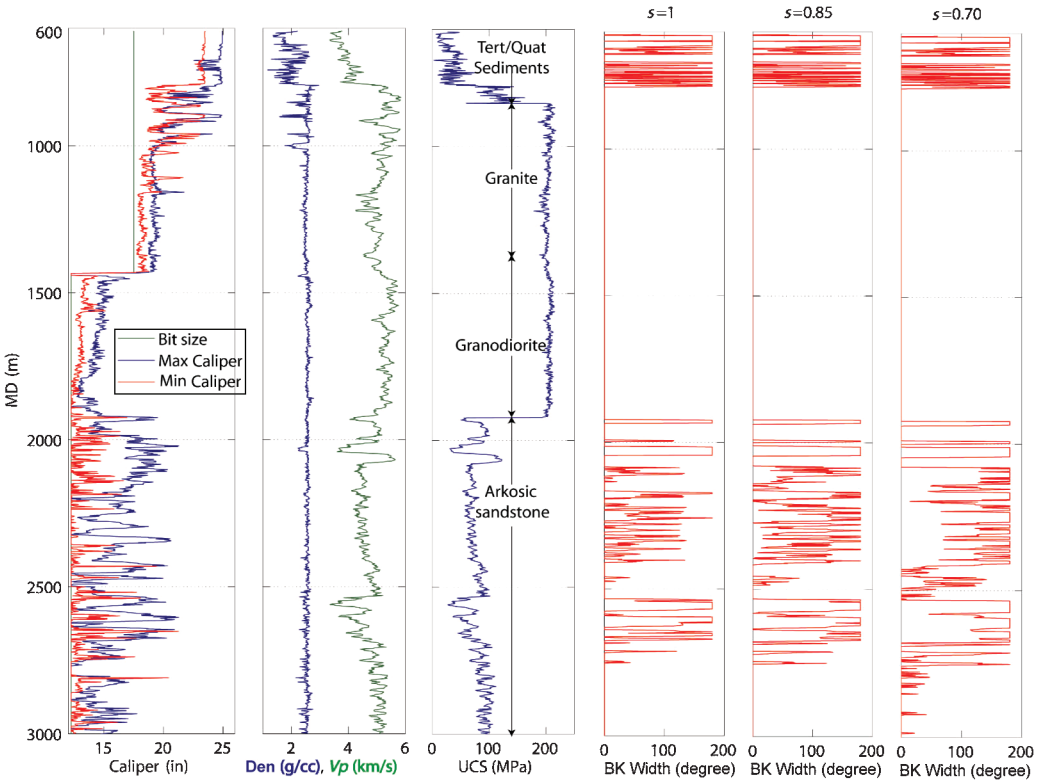

Fig. 9—Column 1: maximum and minimum calipers; Column 2: density and P-wave velocity logs used for rock-strength estimation; Column 3: estimated uniaxial rock strength; Columns 4, 5, and 6: predicted breakout width with used mud weight using *s*=1, *s*=0.85, and *s*=0.7, respectively, in the sedimentary section below 1920 m and *s*=1 for granite, granodiorite, and Tertiary sediments above 1920 m (BK=breakout).

(Columns 4, 5, 6). Overall, we see a very good correlation for $s \approx 0.85$ in the section below 1926 m. The model predicts the observed washouts in the Tertiary sediments at shallow depth. In the granite and granodiorite interval above 1926 m, the borehole was observed to be generally stable, which was predicted by the model. In the sandstone section interval below 1926 m, the breakouts are predicted mostly to be 90 to 120° in width, which generally matches the caliper logs fairly well, although there are some intervals where there is both a predicted and an observed greater amount of failure.

On the basis of the the analysis in the preceding paragraph, the mud weight used during drilling of the deeper sedimentary section in Phase 1 [≈10 pounds per gallon (ppg)] was about 1 ppg less than that, which would have resulted in significantly less hole enlargement **(Fig. 10).** While a modest improvement in wellbore stability would have been achieved with an increase in mud weight of 0.5 ppg, an increase of 1 ppg would have resulted in significant improvements.

Mud-Weight Prediction for Phase 2

By use of the analysis presented, we estimated the mud weight that should be used during Phase-2 drilling in four steps. First, we extrapolated the stress model down to the total depth along the proposed well trajectory. **Fig. 11** shows the modified stress models for S_2 and S_3 based on the observations made during Phase 1. Models for S_1 and P_P (both within and outside the FZ) remain the same as that described by Chéry et al. (2004). Both minifrac tests were performed at the end of Phase 1 at MD of 3028 m, (where $S_3 > S_v + 10$MPa). Two other minifrac tests were performed, one in the vertical section of the well at MD of approximately 1470 m and one at the bottom of hole at 4000 m MD. Both indicate that the stress profile is a classical reverse-/strike-slip fault state (Provost and Houston 2003) outside the FZ as used in the Chéry et al. model (2004). We also assumed that the within the FZ, stresses follow the Chéry et al. model (2004). Then, we used breakout analysis (Fig. 7) between the two minifrac-test intervals outside the FZ to modify

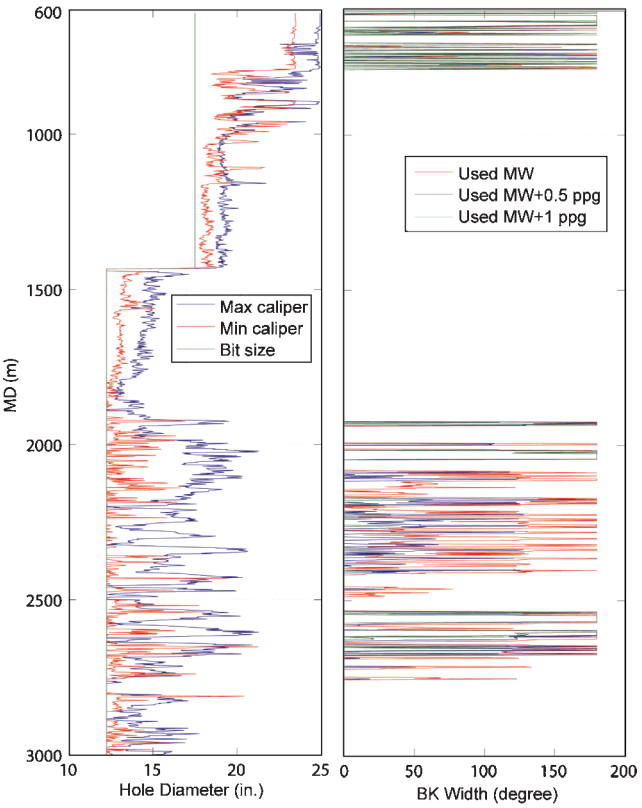

Fig. 10—Column 1: maximum and minimum calipers; Column 2: predicted breakout width with rock strength (for *s*≈0.85) for used mud weight, and mud weights greater by 0.5 ppg and 1 ppg. An increase of ≈1 ppg in mud weight shows significant improvement in the borehole failure (MW=mud weight).

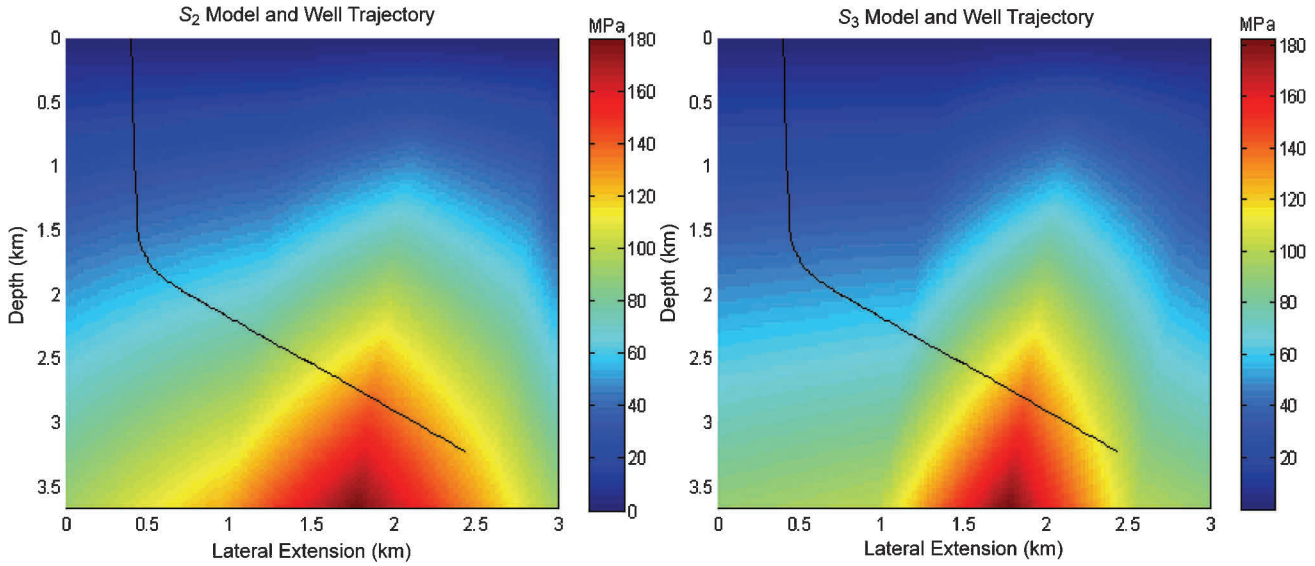

Fig. 11—Modified stress model for principal stresses, S_2 and S_3, through the SAF. Pore pressure and S_1 remain same as Chéry et al. model (2004) (Fig. 6).

the stress profile from the preliminary model. The modified values for S_2 and S_3 (Fig. 11) show increased values of both stresses over a broad region in comparison to the preliminary model. In the second step, we extrapolated rock strength along the well trajectory. To estimate the intact-rock strength using Eq. 2, we used the P-wave velocity data for the rocks to be drilled using a 3D, seismic-tomography model (Thurber et al. 2004). We observed in Phase 1 that an average bulk density of 2.68 g/cm^3 characterized the sedimentary rocks. This value was used for Phase 2. To convert intact-rock strength to in-situ rock strength (incorporating damage to the rocks with varying intensity), we consider a wide range for the factor s in Eq. 3 that goes from 0.5 to 1.0. In other words, we assumed the rock strength was either unaffected by damage ($s=1$) or was reduced by approximately 30% ($s=0.5$). Recall that there was only an 8% decrease ($s=0.85$) in the sedimentary rocks drilled in Phase 1.

The third step of the analysis was to calculate the mud weight required to drill Phase 2, using a range of s values. **Fig. 12** shows the predicted mud weight to prevent borehole failures greater than 60°-breakout width. In fact, this assumption is quite conservative because many wells are drilled successfully with breakout widths that exceed 60°. For the mean case ($s\approx0.74$), the minimum mud weight required to prevent 60° breakout is approximately 11.7 ppg in the FZ and approximately 10.8–11.4 ppg in zones outside the FZ. For weaker rocks ($s\approx0.5$), the required mud weights are approximately 12.3 ppg for the FZ and approximately 11.1 and 12.1 ppg above and below the fault, respectively.

The fourth step of our study was to perform a quantitative risk analysis (QRA) to formally incorporate the uncertainties in the extrapolated stress and rock-strength values. In this way, we could estimate the importance of these parameters for the prediction of minimum mud-weight values.

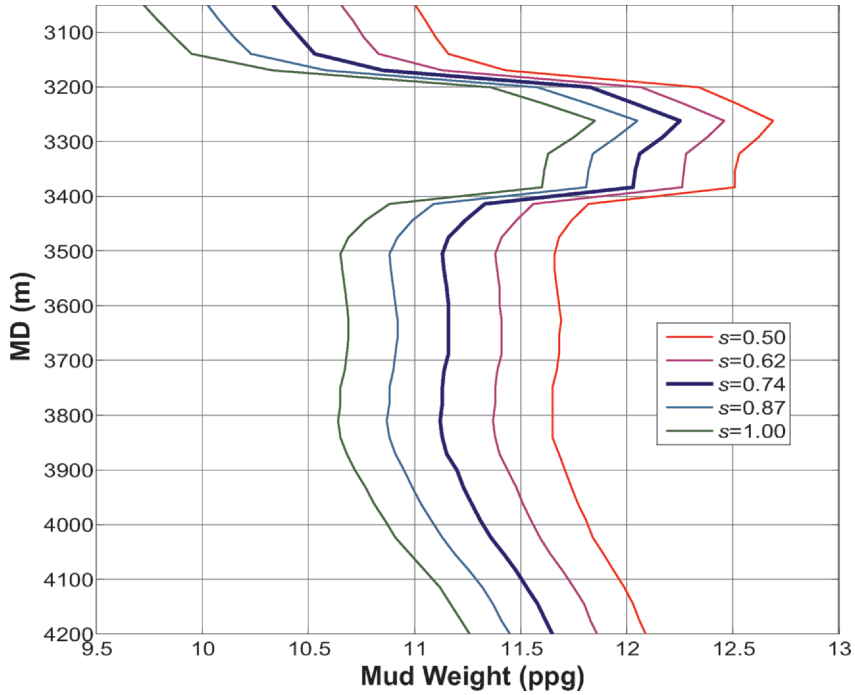

Fig. 12—Mud-weight predictions using estimated rock strength and stress model for 60° breakout width. The analysis shows that a minimum mud weight of approximately 11.2 ppg (no damage, s=1) to 12.3 ppg (30% weaker than undamaged rock, s=0.5) is required to drill through the SAF with a breakout width of≈60°.

QRA To Drill a Stable Borehole Through the SAF

QRA allows us to incorporate uncertainty in the most expected value of the various parameters used in this study to give the probability of success using a particular mud weight (Moos et al. 2003; Ottesen et al. 1999). Analysis will be performed for a maximum breakout width of 60°. We allow for 10% uncertainty in stress magnitudes, a range of azimuths of the maximum horizontal stress between N30°E and N50°E, and a variation of rock strengths that corresponds to values of *s* ranging from 0.5 to 1.0. The QRA shows in **Fig. 13a** that for a mud weight of approximately 11.8 ppg, there is a 50% chance of success (the breakout width not exceeding 60°) in drilling through the SAF (≈3300 m MD). For a mud weight of 12.3 ppg, there is a 90% chance of success. In Fig. 13b we see that rock strength (UCS) defines the uncertainty range of the estimated mud weight to drill a stable borehole with 60º breakout width. Hence, rock strength is the most important parameter in drilling a stable borehole through the FZ. Hence, even with a mud weight of approximately 12 ppg, intervals of extremely weak rock could still be problematic.

Borehole Stability During Phase 2 Through the SAF

Phase-2 drilling and logging showed that the SAF zone (a zone of damaged rock encompassing several currently active fault traces) extends from approximately 3180 to approximately 3420 m. The arkosic sandstones drilled through in the lower part of Phase 1 extend to a depth of 3160 m. Below that depth, the formations encountered were mostly siltstones and claystones associated with the Great Valley formation. These rocks strike subparallel to the SAF and dip mostly to the southwest, such that the wellbore trajectory is roughly orthogonal to the bedding (Boness and Zoback 2006).

The range of mud weights shown in **Fig. 14** was obtained from the QRA to achieve the desired degree of wellbore stability (breakouts that do not exceed 60° width) for the range of uncertainties in *s* illustrated in Fig. 12. As can be seen, this results in a range of recommended mud weights between 10.2 and 12.2 ppg. The mud weights actually used during drilling are also shown in Fig. 14. As can be seen, the initial mud weight was 9.8 ppg, it increased gradually with depth, and it was mostly within the range of mud weights indicated by the analysis described above.

Fig. 14 also shows the vertical and horizontal wellbore diameters as determined from acoustic-caliper data obtained using LWD. LWD data were obtained from 3050 to 3700 m MD, and a problem with the tool resulted in no data from 3550 to 3600 m. Note that at depths above 3630 m, the hole is in good shape. The horizontal diameter is very close to the bit size, and the vertical dimension shows only modest increases in hole size at a few depths. Hence, the mud weight predicted using the analysis did a good job of maintaining wellbore stability during drilling of most of the interval shown.

Another source of data that confirms this conclusion is the volume of mud in the hole as it was being drilled **(Fig. 15).** Hole volume is calculated assuming a cylindrical-shaped borehole with variable diameter, and it is defined by calipers with MD. Mud volume is estimated by correcting the hole volume for the volume of drilling assembly in the hole. Note that the actual mud volume is the same as that predicted for an in-gauge hole to approximately 3450 m MD. However, the cumulative hole volume calculated from the LWD caliper data below 3450 m show that the hole volume should have been essentially equivalent to that corresponding to an in-gauge hole to 3550 m. This implies that the increase in hole volume seen in the interval between 3450 and 3550 m MD was occurring higher up the hole because the acoustic caliper is

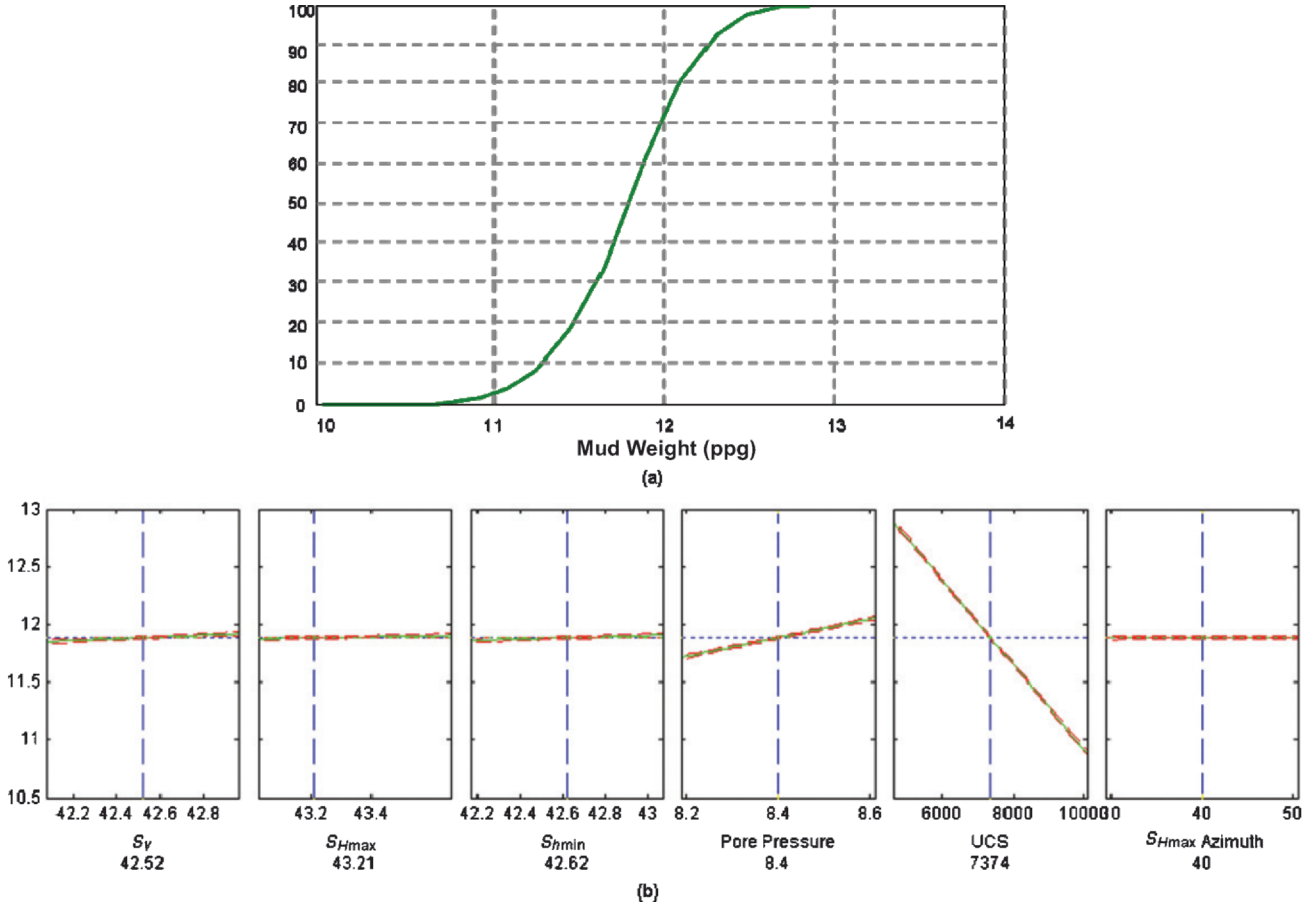

Fig. 13—(a) QRA at the SAF zone (≈3300 m)—the probability of success (to drill with 60° breakout width) as a function of mud weight. (b) The sensitivity analysis shows rock strength is the most sensitive parameter controlling the mud weight required to drill a stable hole through the fault zone. Stress and pore pressure are in ppg. UCS is in psi, and S_{Hmax} azimuth is in degrees.

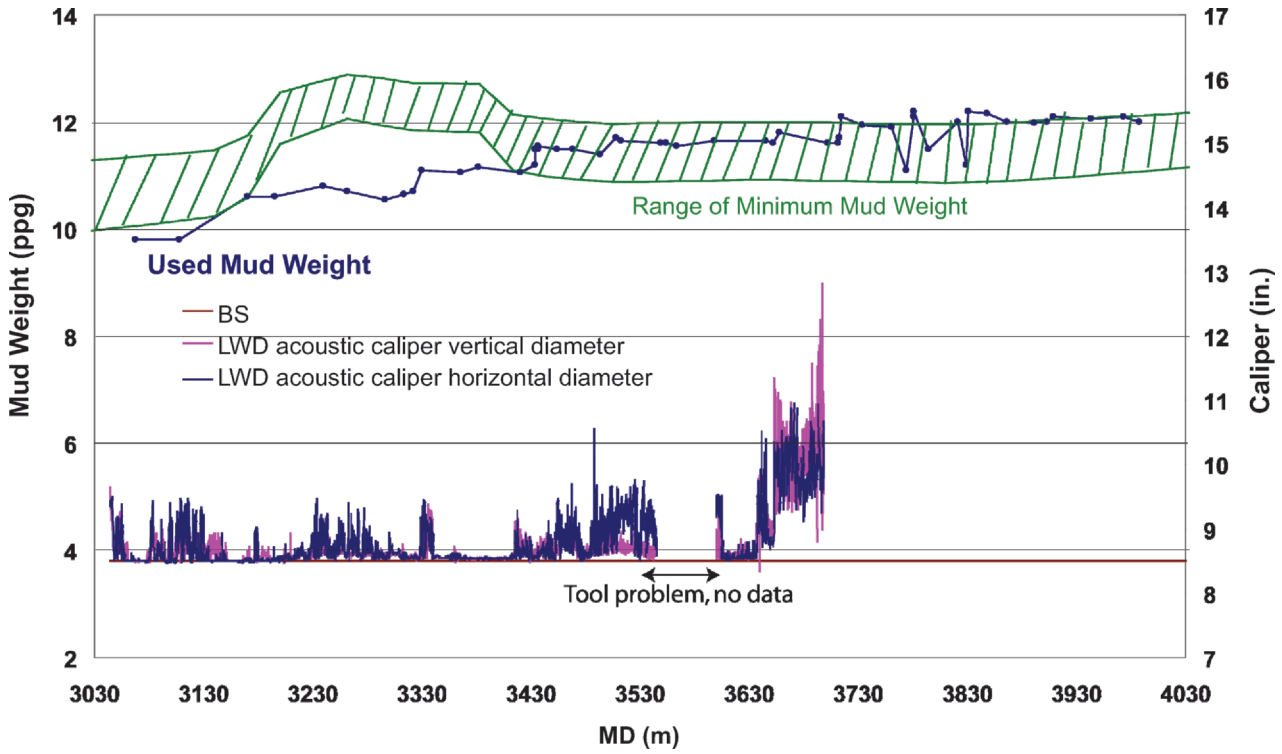

Fig. 14—Through the SAF, LWD acoustic calipers show relatively little borehole failure in Phase-2 drilling when drilled with a mud weight close to predicted mud weight. Below 3650 m, LWD shows onset of significant failure.

located only 14 m above the bit. Hence, there seems to be a degree of time-dependent failure of the hole at depths above 3450 m, while at the same time, the hole was in gauge as it was being drilled from 3450 to 3550 m. Time-dependent hole failure is discussed in more detail in the Time-Dependent Failure section.

Between 3640 m and 3700 m MD, the acoustic-caliper data (and hole-volume data) show the onset of significant hole enlargements. In the acoustic caliper data, a moderate washout (approximately 2–3 in.) is observed (Fig. 14). In the hole-volume data (Fig. 15), we see an increase of volume with depth in excess of that expected if the hole were in gauge. Hence, we seem to be using a mud weight that is too low. One reason for this might be the fact that because the SAF was crossed at MD of approximately 3300 m (TVD of approximately 2800 m), the strength analysis described, which was based on the sedimentary section drilled during Phase 1 to the southwest of the SAF, might have resulted in an underestimate of the strength of the Great Valley formation on the northeast side of the fault.

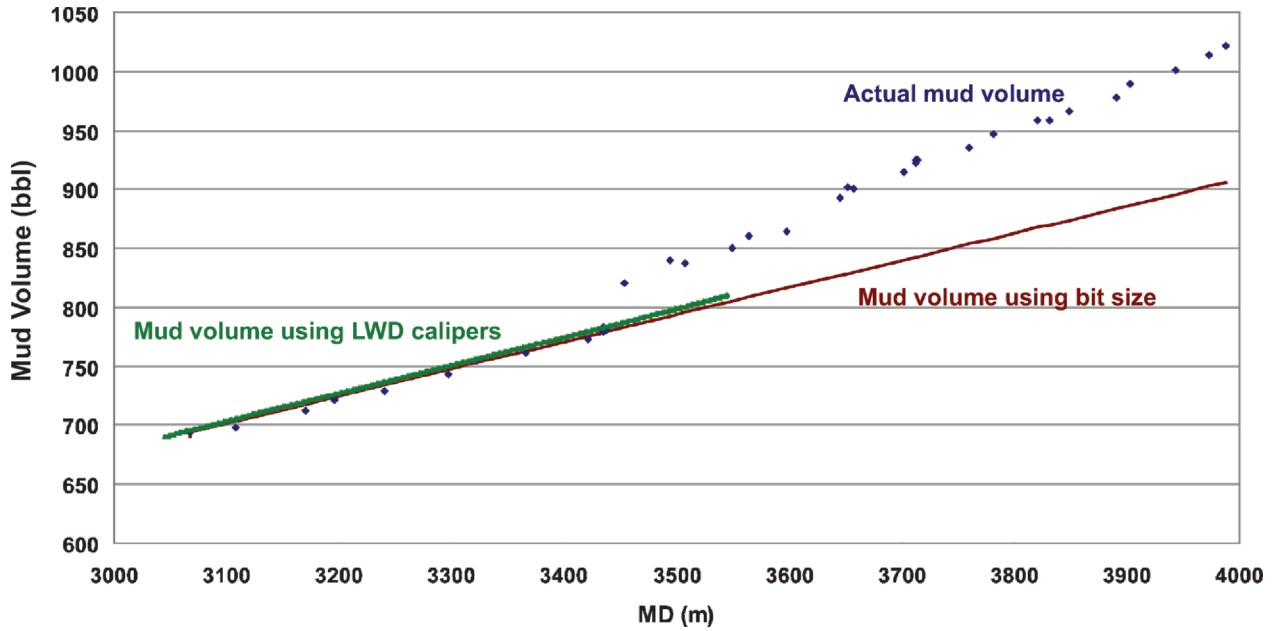

Fig. 15—A good match of the actual mud volume to estimated mud volume from the bit size and the LWD calipers indicates that the hole was relatively in good shape while drilling for the interval above 3440 m. LWD mud volume indicates good hole till 3550 m MD, while deviation of the actual mud volume from the bit-size mud volume at this interval suggests time-dependent failures at an interval above 3550 m. Higher actual-mud-volume slope than bit-size mud-volume slope indicates onset of significant hole failure below 3550 m.

Time-Dependent Failure

Once Phase-2 drilling was completed at a MD of 3980 m, a six-arm-caliper log was run **(Fig. 16).** Surprisingly, this log showed very large hole enlargements, even in the interval from 3050 to 3650 m where the LWD (and hole-volume) data show that the hole was in gauge as it was being drilled. Thus, the enlarged calipers indicate deterioration of the borehole with time. Time-dependent hole failure is clear for the depths covered by the LWD data, as is shown by a direct comparison between Figs. 15 and 16. The time-dependent failure of the borehole was so severe that some depth intervals one (or two) of the calipers were fully extended. As shown in the inset in the upper right of Fig. 16 (a superposition of all the caliper data looking down the hole), the borehole seems to be enlarged primarily on the top of the hole. The blue symbols represent the tool position in the hole, determined by using the algorithm described by Jarosinski (1998). The fact that the hole enlargements appear to be on the top of the hole might, in part, be an artifact of the logging tool being near the bottom of the deviated well and might, in part, result from the fact that the hole failure might have caused there to be a cuttings bed on the bottom of the hole.

One possible process responsible for the time-dependent hole failure is that time-dependent chemical reactions between the water-based mud and the clays in shaly rocks decreased rock strength with time. However, the time-dependent increase in hole size is seen over the entire depth range drilled in Phase 2, including the arkosic rocks extending to 3180 m. Moreover, such interactions are not known to be a significant problem in the many oil and gas wells drilled with water-based mud in the Great Valley formation in the region. The most likely possibility is time-dependent mud penetration into the rock surrounding the borehole. Fluid penetration around the well would increase pore pressure, reduce the effectiveness of mud weight to stabilize the hole, and could cause cavitation of the rock surrounding the wellbore.

Fig. 17 shows LWD-caliper and -resistivity logs with multiple depths of investigation (Tracks 1 and 2, from left to right) and wireline-caliper and -resistivity logs that were measured after several days of LWD logs when drilling was completed (Tracks 3 and 4). There is almost no separation in LWD-resistivity logs, but wireline-resistivity logs from different depths of investigation are separated, indicating mud-fluid penetration into the formation with time probably because of the numerous fractures in these formations. Below 3750 m MD in Fig. 17, the post-drilling wireline-caliper data indicate that the hole is less enlarged, which matches the minimal separation between the resistivity logs. This likely happened because of the low permeability of the formations and the fact that there was insufficient time for mud fluid to penetrate into the formation.

Modeling of Time-Dependent Failure

In this section, we present a FEM exercise to investigate mud penetration into the formation (and the change of pore pressure) immediately surrounding the wellbore with time. Increase in the pore pressure promotes both failure of the intact rock and shear failure on fracture planes, both of which lead to enlargement of the borehole.

An FEM schematic model **(Figs 18a and b)** of the near-wellbore region is shown in Fig. 18a. We use realistic values for fracture permeability (≈1 md) and matrix permeability (≈0.004 md) for tight sandstones (Dürrast et al. 2002). The borehole mud pressure of approximately 33 MPa (used during drilling) and formation pore pressure of approximately 29 MPa (estimated by in-situ measurements) are used as initial boundary conditions for the modeling.

Modeling of the pressure-diffusion process indicates that mud starts penetrating the relatively high-permeability fractures and gradually spreads out around the borehole with time. Hence, the initial shape of the diffusion front is dependent on the number of fractures and their intersecting locations with the borehole. The modeling shows the first sign of pressure change around the borehole at approximately 3 hours **(Fig. 19a).** Figs. 19b, c, and d show pressure changes after 2 days, 2 weeks, and 4 weeks, respectively. It illustrates that it takes 2 to 4 weeks for the pressure front to spread approximately 10–12 in. from the borehole wall, which is consistent with the rate of time-dependent failure observed in the SAFOD borehole.

Incorporating the pressure changes shown in Fig. 19d into a 3D model of potential wellbore failure demonstrates that, after approximately 4 weeks, one would expect a large zone of failure around the wellbore (reddish zone in Fig. 18b). For a symmetric distribution of fractures, the shape of the increased-pore-pressure area, where fracture planes may slip, is symmetric around the borehole. However, observed failures seem to be mostly on the top of the borehole (Fig. 16 insert). Because of the high deviation angle of the well, removable blocks from the top section of the hole fall into the hole, but this would not happen for failing blocks

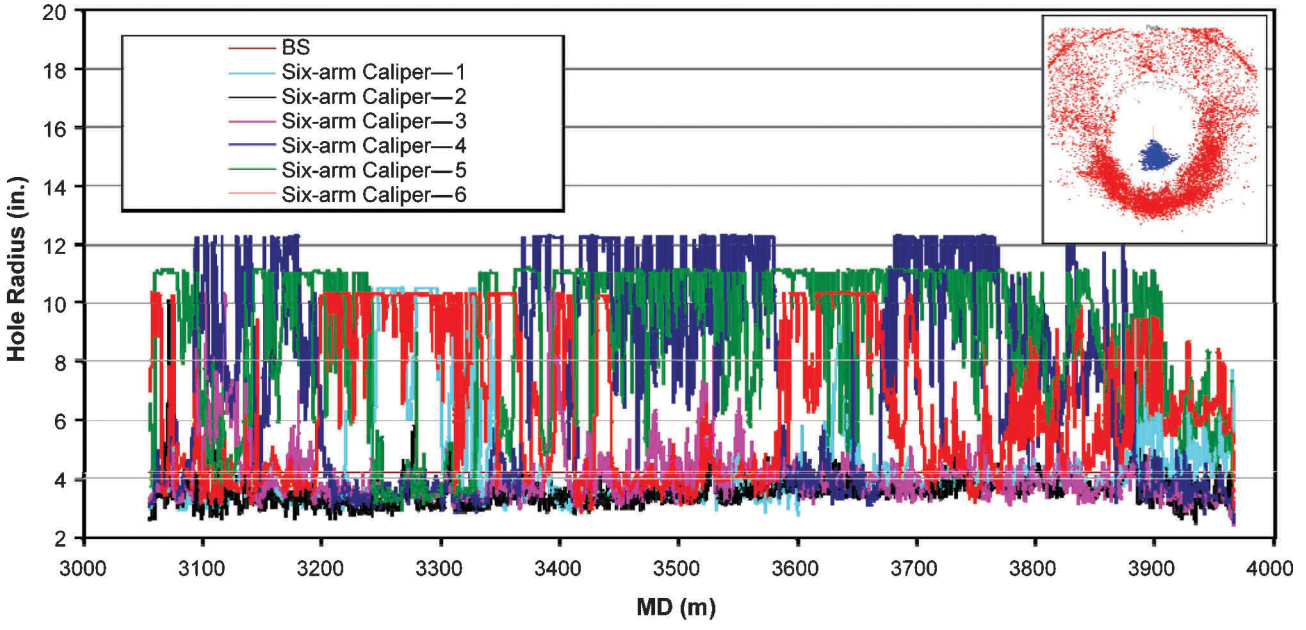

Fig. 16—Six-arm wireline calipers show deterioration of the borehole with time. In the right upper corner, centralized six-arm caliper pads are plotted in a borehole coordinate system. Borehole shape is highly extended at the top and top corners, indicating failure in weak planes with time because of mud penetration.

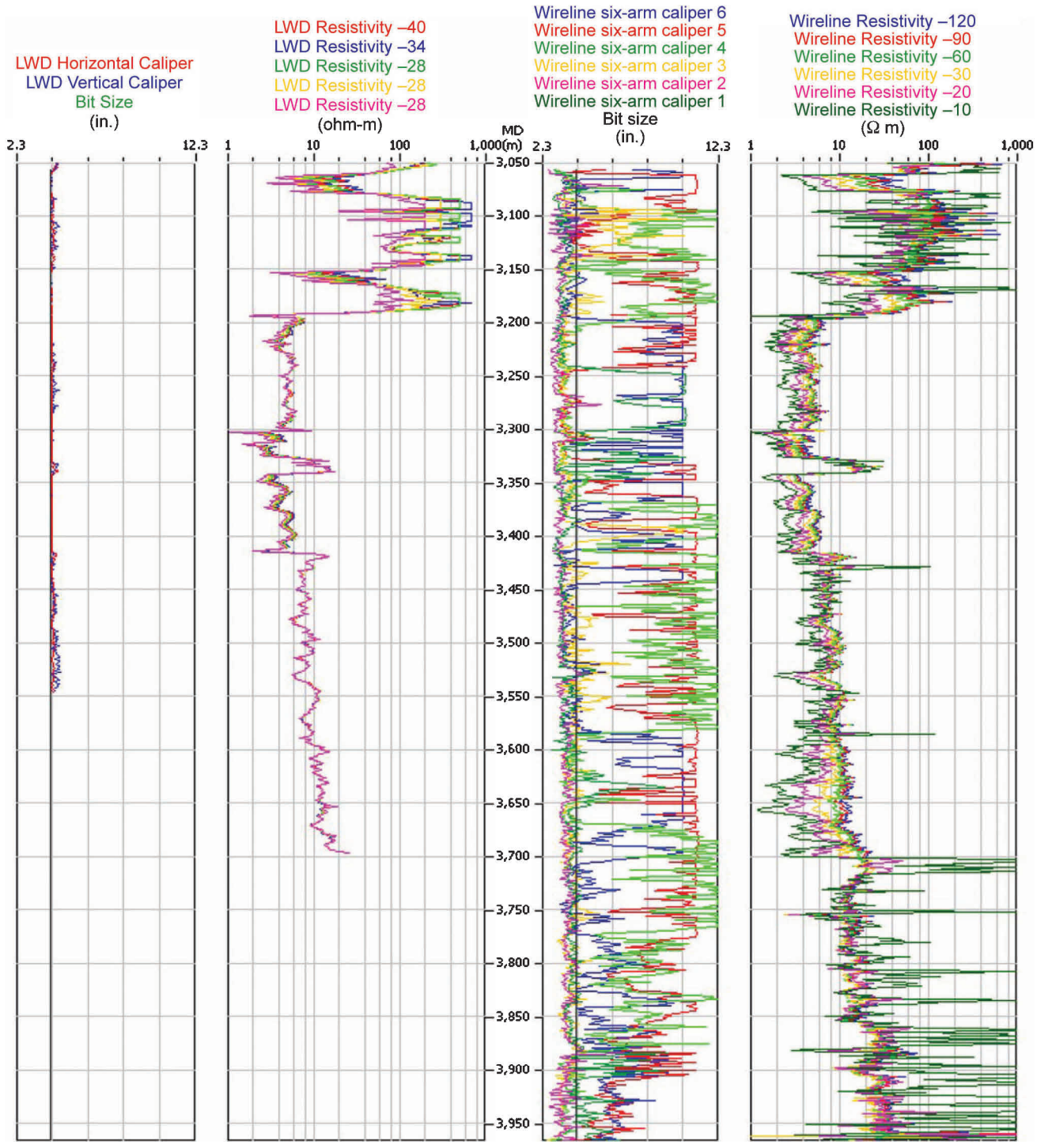

Fig. 17—LWD-caliper (Track 1, far left) and -resistivity logs (Track 2) with multiple depths of investigation indicate a stable borehole and no fluid penetration around the borehole. Wireline-resistivity logs (Track 4) measured a few days after the LWD logs show separation between them, indicating mud penetration into the formation, which may cause failure in the borehole as observed by the wireline calipers (Track 3).

adjacent to the bottom of the hole, thus leading to the appearance of asymmetric failure. The apparent asymmetry of the failure zone around the well is also enhanced by the accumulation of the failed material (a cuttings bed developed) on the bottom of the hole.

Conclusions

This study defines a generalized workflow that could be applicable for wellbore-stability analysis of wells located in areas with a complex stress field and little information about the rock strength. Using the predicted mud weights of approximately 10.5–12.5 ppg, the SAFOD borehole was drilled successfully through the SAF with relatively little failure (as indicated by LWD-caliper and hole-volume data). Six-arm-caliper data collected after drilling showed significant increases in the size of the borehole with time, which is most likely caused by mud penetration around the well. Mud penetration is indicated by the separation in the resistivity logs (run along with six-arm caliper) with multiple depths of investigation. FEM shows that penetration of the drilling mud into the rocks surrounding the wellbore is a slow process, which explains the time dependency of the wellbore instability. Once the pore pressure in these bedded and fractured rocks crosses the threshold for shearing the fracture planes, failure occurs. Asymmetry in the

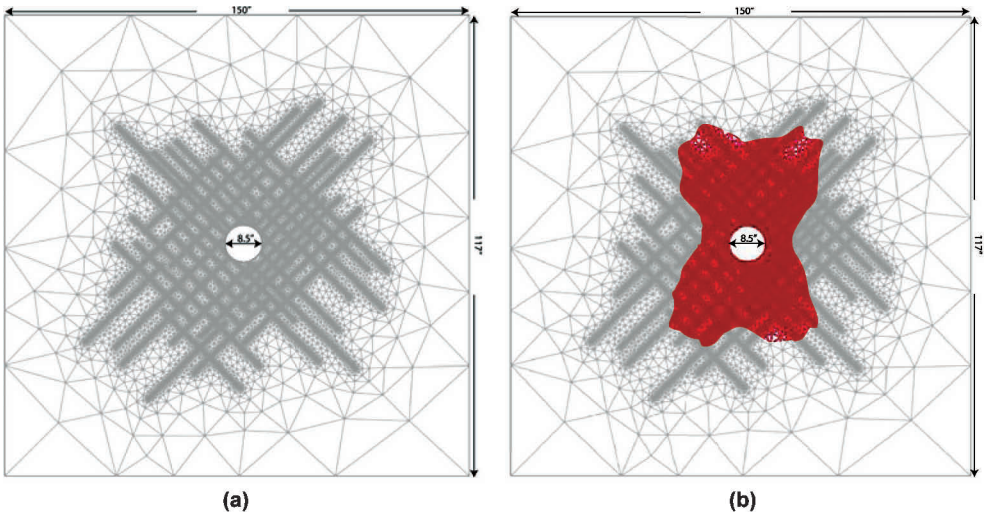

Fig. 18—(a) A triangular mesh of the schematic model for the near-wellbore region around the borehole. Permeability values of 1 md and 0.004 md are used for fracture and matrix, respectively. Mud pressure and pore pressure are kept at 33 MPa and 29 MPa, respectively. (b) Red zone indicates zone of failure around the borehole because of mud invasion.

shape of the failed wellbore is mostly coming from the fact that the SAFOD borehole is highly deviated (≈54°); so, failed blocks at the bottom of the borehole cannot be removed. This effect is enhanced by accumulation of debris falling from the top and by an artifact introduced by the tool lying at the bottom of the hole.

Nomenclature

P_p = pore pressure
s = weaking parameter to estimate jointed-mass rock strength from intact rock strength
S_1 = first (maximum) principal stress
S_2 = second principal stress
S_3 = third (minimum) principal stress
$S_{H\max}$ = maximum principal horizontal stress
$S_{h\min}$ = minimum principal horizontal stress
S_v = vertical stress
T = time
V_p = velocity of P-wave
ρ = bulk density of medium

Acknowledgments

The SAFOD project is part of the EarthScope initiative of the US National Science Foundation, which is being carried out in col-

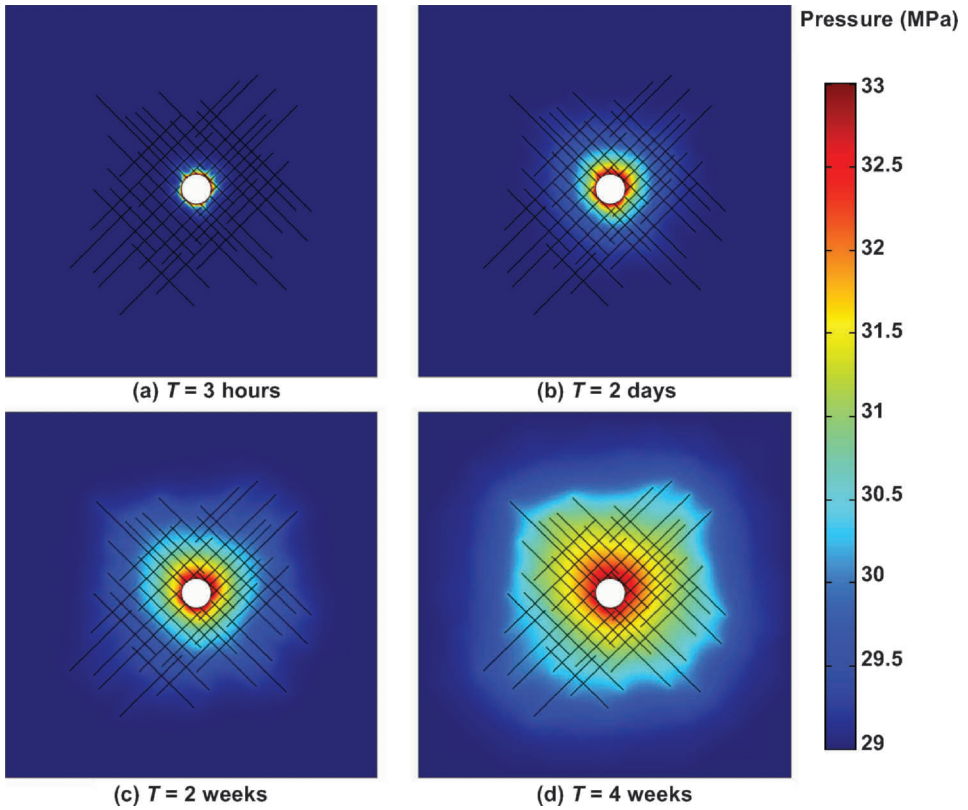

Fig. 19—Pressure front at (a) 3 hours, (b) 2 days, (c) 2 weeks, and (d) 4 weeks, indicating that it takes approximately 2 to 4 weeks for the front to spread a mud weight of approximately 33 MPa to approximately 10–12 in. from the borehole wall by the diffusion process (scale same as Fig. 18).

laboration with the US Geological Survey. Financial, engineering, and technical help from the International Continental Drilling Program is gratefully acknowledged. The Stanford Rock and Borehole Geophysics Consortium funded this project. We would like to acknowledge the scientists and engineers of the SAFOD team for their contribution to the success of the project. We also thank GeoMechanics International for the use of its software in carrying out this study.

References

Anderson, E.M. 1951. *The dynamics of faulting and dyke formation with applications to Britain*, second edition. Edinburg, UK: Oliver and Boyd.

Annor, A. and Jackson, R. 1987. Mechanical, thermal and joint properties of rock samples from the Lac du Bonnet Batholith, Manitoba. In *Geotechnical Studies at Whiteshell Research Area (RA-3)*, ed. T.J. Katsube and J.P. Jume. Ottawa, Canada: Div. Rep. MRL 87-52, CANMET Min. Res. Lab.

Boness, N. and Zoback, M.D. 2006. A multiscale study of the mechanisms controlling shear velocity anisotropy in the San Andreas Fault Observatory at Depth. *Geophysics* **71** (5): 131–146. DOI:10.1190/1.2231107.

Brune, J.N., Henyey, T.L., and Roy, R.F. 1969. Heat flow, stress, and rate of slip along the San Andreas Fault, California. *J. Geophys. Res.* **74** (15): 3821–3827. DOI:10.1029/JB074i015p03821.

Chang, C., Zoback, M.D., and Khakasar, A. 2006. Empirical relations between rock strength and physical properties of sedimentary rocks. *J. Pet. Sci. Eng.* **51** (3–4): 223–237. DOI:10.1016/j.petrol.2006.01.003.

Chéry, J., Zoback, M.D., and Hickman, S. 2004. A mechanical model of the San Andreas fault and SAFOD Pilot Hole stress measurements. *Geophys. Res. Lett.* **31** (L15S13). DOI:10.1029/2004GL019521.

Chirkov, S.E., Popov, V.N., and Mirzoyan, A.A. 1979. Determination of the strength characteristics of jointed rocks in situ. *Journal of Mining Science* **15** (5): 453–456.

Dürrast, H., Rasolofosaon, P.N.J., and Siegesmund, S. 2002. *P*-wave velocity and permeability distributions of sandstones from a fractured tight gas reservoir. *Geophysics* **67** (1): 241–253. DOI:10.1190/1.1451673.

Goodman, R.E. 1989. *Introduction to Rock Mechanics*, second edition, 257–280. New York: John Wiley and Sons.

Goodman, R.E., and Shi, G. 1985. *Block Theory and It's Application to Rock Engineering*. Englewood Cliffs, New Jersey: International Series in Civil Engineering and Engineering Mechanics, Prentice-Hall.

Hickman, S. and Zoback, M.D. 2004. Stress orientations and magnitudes in the SAFOD Pilot Hole. *Geophys. Res. Lett.* **31** (L15S12). DOI:10.1029/2004GL020043.

Hoek, E. and Brown, E.T. 1980. Empirical strength criteria for rock masses. *J. Geotech. Eng. Div., ASCE* **106** (GT9): 1013–1035.

Hoek, E. and Brown, E.T. 1997. Practical estimates of rock mass strength. *Int. J. Rock Mech. Min. Sci.* **34** (8): 1165–1186. DOI:10.1016/S1365-1609(97)80069-X.

Hongliang, H. and Ahrens, T.J. 1994. Mechanical properties of shock-damaged rocks. *Int. J. Rock Mech. Min. Sci. & Geomech. Abstr.* **31** (5): 525–533. DOI:10.1016/0148-9062(94)90154-6.

Hu, K.X. and Huang, Y. 1993. Estimation of the elastic properties of fractured rock masses. *Int. J. Rock Mech. Min. Sci. & Geomech. Abstr.* **30** (4): 381–394. DOI:10.1016/0148-9062(93)91721-T.

Jaeger, J.C. 1970. Behavior of closely jointed rock. In *Rock Mechanics—Theory and Practice: Eleventh Symposium on Rock Mechanics*, 57–68. New York: Society of Mining Engineers of AIME.

Jarosinski, M. 1998. Contemporary stress field distortion in the Polish part of the Western Outer Carpathians and their basement. *Tectonophysics* **297** (1–4): 91–119. DOI:10.1016/S0040-1951(98)00165-6.

Lachenbruch, A.H. and Sass, J.H. 1980. Heat flow and energetics of the San Andreas Fault zone. *J. Geophys. Res.* **85** (B11): 6185–6222. DOI:10.1029/JB085iB11p06185.

Moos, D., Peska, P., Finkbeiner, T., and Zoback, M.D. 2003. Comprehensive wellbore stability analysis using Quantitative Risk Assessment. *J. Petrol. Sci. and Eng.* **38** (3–4): 97–109. DOI:10.1016/S0920-4105(03)00024-X.

Moos, D., Zoback, M.D., and Bailey, L. 2001. Feasibility Study of the Stability of Openhole Multilaterals, Cook Inlet, Alaska. *SPEDC* **16** (3): 140–145. SPE-73192-PA. DOI: 10.2118/73192-PA.

Mount, V.S. and Suppe, J. 1987. State of stress near the San Andreas Fault: Implications for wrench tectonics. *Geology* **15** (12): 1143–1146. DOI:10.1130/0091-7613(1987)15<1143:SOSNTS>2.0.CO;2.

Ottesen, S., Zheng, R.H., and McCann, R.C. 1999. Wellbore stability assessment using quantitative risk analysis. Paper SPE 52864 presented at the SPE/IADC Drilling Conference, Amsterdam, 9–11 March. DOI: 10.2118/52864-MS.

Peska, P. and Zoback, M.D. 1995. Compressive and tensile failure of inclined well bores and determination of in situ stress and rock strength. *J. Geophys. Res.* **100** (B7): 791–811. DOI:10.1029/95JB00319.

Provost, A.-S. and Houston, H. 2003. Stress orientations in northern and central California: Evidence for the evolution of frictional strength along the San Andreas plate boundary system. *J. Geophys. Res.* **108** (B3): 2175. DOI:10.1029/2001JB001123.

Rice, J.R. 1992. Fault stress states, pore pressure distributions, and the weakness of the San Andreas Fault. In *Fault Mechanics and Transport Properties of Rocks*, ed. B. Evans and T-F. Wong, 475–503. London: Academic Press.

Schlumberger. 2004. *FMI Fullbore Formation MicroImager*, FE_04_019_0. Marketing Communications, Houston (August 2004).

Selby, M.J. 1980. A rock mass strength classification for geomorphicological purposes: with tests from Antarctica and New Zealand. *Zeitschrift für Geomorphologie* **24:** 31–51.

Thurber, C., Roecker, S., Zhang, H., Baher, S., and Ellsworth, W. 2004. Fine-scale structure of the San Andreas Fault zone and location of the SAFOD target earthquakes. *Geophys. Res. Lett.* **31** (L12S02). DOI:10.1029/2003GL019398.

Townend, J. and Zoback, M.D. 2004. Regional tectonic stress near the San Andreas fault in central and southern California. *Geophys. Res. Lett.* **31** (L15S11). DOI:10.1029/2003GL018918.

Unsworth, M. and Bedrosian, P.A. 2004. Electrical resistivity structure at the SAFOD site from magnetotelluric exploration. *Geophys. Res. Lett.* **31** (L12S05). DOI:10.1029/2003GL019405.

Zoback, M.D. 2006. SAFOD penetrates the San Andreas Fault. *Scientific Drilling* **2** (March 2006): 32–33. DOI:10.2204/iodp.sd.2.07.2006.

Zoback, M.D. 2007. *Reservoir Geomechanics*, 84–137. Cambridge, UK: Cambridge University Press.

Zoback, M.D., Barton, C., Brudy, M., Castillo, D., Finkbeiner, T., Grollimund, B., Moos, D., Peska, P., Ward, C., and Wiprut, D. 2003. Determination of stress orientation and magnitude in deep wells. *Int. J. Rock Mech. Min. Sci.* **40** (7–8): 1049–1076. DOI:10.1016/j.ijrmms.2003.07.001.

Zoback, M.D., Hickman, S., and Ellsworth, W. 2007. The Role of Fault Zone Drilling. In *Treatise on Geophysics Volume 4: Earthquake Seismology*, ed. G. Schubert and H. Kanamori, Section 4.22, 649–674. Amsterdam: Elsevier.

Zoback, M.D., Zoback, M.L., Mount, V.S., Suppe, J., Eaton, J.P., Healy, J.H., Oppenheimer, D. et al. 1987. New evidence on the state of stress of the San Andreas fault system. *Science* **238** (4830): 1105–1111. DOI:10.1126/science.238.4830.1105.

SI Metric Conversion Factors

bbl × 1.589 873	E–01 = m^3
ft × 3.048*	E–01 = m
in. × 2.54*	E–02 = m
ppg × 2.245 322*	E–02 = SG
psi × 6.894 757	E–03 = MPa

* Conversion factor is exact.

Pijush Paul works in the reservoir structure team of ConocoPhillips Subsurface Technology Group in Houston. email: pijush.k.paul@conocophillips.com. His current projects focus

on providing geomechanical models of reservoirs for completion and production optimization. He is also active in the team's computational geomechanics program. Paul holds a PhD degree in geophysics, and an MS degree in petroleum engineering from Stanford University. He also holds an MT degree in applied geophysics from the Indian Institute of Technology and a BS degree in geology and physics from St. Xavier's College in India. **Mark Zoback** has been a professor of geophysics at Stanford University since 1984. His principal research interests are related to the forces that act within the earth's crust and their influence on processes related to plate tectonics, earthquakes, and oil and gas reservoirs. He has authored, or coauthored, approximately 250 technical papers and is the author of the technical reference book *Reservoir Geomechanics*, published in 2007 by Cambridge University Press.